

An enquiry on the origins of N-rich stars in the inner Galaxy based on APOGEE chemical compositions

Shobhit Kisku^{1*}, Ricardo P. Schiavon¹, Danny Horta¹, Andrew Mason¹,
J. Ted Mackereth^{2,3}, Sten Hasselquist^{4,5}, D. A. García-Hernández^{6,7},
Dmitry Bizyaev^{8,9}, Joel R. Brownstein⁴, Richard R. Lane¹⁰, Dante Minniti¹¹,
Kaïke Pan⁸, Alexandre Roman-Lopes¹²

¹*Astrophysics Research Institute, Liverpool John Moores University, 146 Brownlow Hill, Liverpool L3 5RF, UK*

²*Canadian Institute for Theoretical Astrophysics, University of Toronto, 60 St. George Street, Toronto, ON M5S 3H8, Canada*

³*Dunlap Institute for Astronomy and Astrophysics, University of Toronto, 50 St. George Street, Toronto, ON M5S 3H4, Canada*

⁴*Department of Physics and Astronomy, University of Utah, 115 S. 1400 E., Salt Lake City, UT 84112, USA*

⁵*NSF Astronomy and Astrophysics Postdoctoral Fellow*

⁶*Instituto de Astrofísica de Canarias (IAC), E-38205 La Laguna, Tenerife, Spain*

⁷*Universidad de La Laguna (ULL), Departamento de Astrofísica, E-38206 La Laguna, Tenerife, Spain*

⁸*Apache Point Observatory and New Mexico State University, P.O. Box 59, Sunspot, NM, 88349-0059, USA*

⁹*Sternberg Astronomical Institute, Moscow State University, Moscow*

¹⁰*Instituto de Astronomía y Ciencias Planetarias de Atacama, Universidad de Atacama, Copayapu 485, Copiapó, Chile*

¹¹*Instituto de Astrofísica, Pontificia Universidad Católica de Chile, Av. Vicuña Mackenna 4860, 782-0436 Macul, Santiago, Chile*

¹²*Departamento de Física, Facultad de Ciencias, Universidad de La Serena, Cisternas 1200, La Serena, Chile*

Accepted XXX. Received YYY; in original form ZZZ

ABSTRACT

Recent evidence based on APOGEE data for stars within a few kpc of the Galactic centre suggests that dissolved globular clusters (GCs) contribute significantly to the stellar mass budget of the inner halo. In this paper we enquire into the origins of tracers of GC dissolution, N-rich stars, that are located in the inner 4 kpc of the Milky Way. From an analysis of the chemical compositions of these stars we establish that about 30% of the N-rich stars previously identified in the inner Galaxy may have an accreted origin. This result is confirmed by an analysis of the kinematic properties of our sample. The specific frequency of N-rich stars is quite large in the accreted population, exceeding that of its *in situ* counterparts by near an order of magnitude, in disagreement with predictions from numerical simulations. We hope that our numbers provide a useful test to models of GC formation and destruction.

Key words: Globular Clusters: general – Galaxy: formation – Galaxy: bulge – Galaxy: kinematics and dynamics – Galaxy: abundances

1 INTRODUCTION

One of the main consequences of the current cosmological paradigm, Lambda Cold Dark Matter (Λ -CDM), is that galaxies grow through the process of hierarchical mass assembly, whereby smaller galaxies are accreted to form larger more massive systems. Such theoretical predictions are in line with the identification of phase-space substructures residing in the Galactic stellar halo, such as Gaia-Enceladus/Sausage (GE/S, [Belokurov et al. 2018](#); [Haywood et al. 2018](#); [Helmi et al. 2018](#); [Mackereth et al. 2019](#)) and Sequoia ([Myeong et al. 2019](#)). As well as halo stellar streams ([Helmi et al. 1999](#); [Ibata et al. 2016](#); [Belokurov et al. 2018](#)) and ongoing accre-

tion, such as the Sagittarius dwarf spheroidal (Sgr dSph, [Ibata et al. 1994](#)). The longer dynamical timescales of less dense regions, such as the outer halo, preserves phase-space information and therefore allows the reconstruction of the integrals of motion (IOM) of these accreted systems. The situation is not as simple in the inner halo due to the shorter dynamical timescales. Moreover, large extinction towards the inner Galaxy and crowding by more massive metal-rich Galactic components, such as the thick and thin disk, and the bar, make observational access to the inner halo difficult. These difficulties have recently been overcome by the APOGEE survey ([Majewski et al. 2017](#)), which obtained detailed chemistry based on NIR spectroscopy for over 10^4 stars in the inner Galaxy, leading up to the discovery of a large population of N-rich stars within a few

* E-mail: S.S.Kisku@2015.ljmu.ac.uk

kpc of the Galactic centre, and the recent identification of Heracles (Horta et al. 2021a).

In addition to phase-space substructure, stellar streams and ongoing accretion events in the Galactic stellar halo, ancient Globular Clusters (GC) are also thought to contribute relevantly to the total stellar halo mass budget (Martell et al. 2016; Schiavon et al. 2017; Koch et al. 2019; Reina-Campos et al. 2020; Hughes et al. 2020; Horta et al. 2021b). Such contribution arises from the dissolution and/or evaporation of GCs, which are disrupted via different processes (e.g. tidal shocks, evaporation and disruption by encounters with massive molecular clouds, Gnedin 2001; Elmegreen 2010; Kruijssen et al. 2011), so that stars resulting from GC dissolution can be found in the field of the stellar halo.

Detection of the remnants of GC dissolution in the field is made possible by the presence of stars with chemically peculiar chemical compositions in GCs. These systems have been found to host multiple stellar populations with distinct abundance patterns (for a detailed description, see a review by Bastian & Lardo 2018). Stars that display the same abundances patterns as the field population are dubbed "First Generation" (FG) stars, whereas those that show enhancements in He, N and Na, and show lower O and C are referred to as "Second Generation" (SG) stars. Since abundance patterns of FG stars are indistinguishable from those of field populations, stars with abundance patterns typical of SG population are used as tracers of the contribution of dissolved GCs to the stellar mass budget of the Galaxy.

Field stars that display abundance patterns typical of SG GC stars have been identified in the stellar halo by several groups (Martell & Grebel 2010; Lind et al. 2015; Martell et al. 2016; Koch et al. 2019; Tang et al. 2019, 2020). Using APOGEE DR12 data, Schiavon et al. (2017) identified a large population of N-rich stars in the inner $\sim 2\text{--}3$ kpc from the Galactic centre. Based on more recent data releases, these enriched stars have been identified out to large distances up to ~ 15 kpc by Horta et al. (2021b). The large population of N-rich stars identified by Schiavon et al. (2017) is suggested to contribute a minimum of 19–25% to the stellar mass in the inner ~ 2 kpc of the halo¹. Looking at the halo stars with $|z| > 10$ kpc, Martell et al. (2016) find the contribution to the stellar mass budget due to GC dissolution to be $\sim 2\%$. Such a large spatial variation of the frequency of N-rich stars has been quantified by Horta et al. (2021b). By taking into account the APOGEE selection effects, they measure a ratio of $\sim 17^{+10}_{-7}\%$ and $\sim 3^{+1}_{-0.8}\%$ at $R_{GC} \sim 1.5$ kpc and $R_{GC} \sim 15$ kpc, respectively.

With the availability of *Gaia*'s high-quality parallaxes and the resulting 6D phase-space information, orbital parameters and IOM for Milky Way stars can be estimated. Since these properties are essentially invariant in low density regions of the Milky Way, they can be used to group stars according to orbital properties that are associated to those of the progenitor system. Recent studies concerning the origins of enriched stars in the halo which show similar abundances to those of SG GCs have investigated the likelihood that these enriched stars originate from GCs (Carollo et al. 2013; Savino & Posti 2019; Tang et al. 2020; Hanke et al. 2020). Savino & Posti (2019) directly compare the IOM of 57 CN-strong field stars, observed in SEGUE and SEGUE-2 surveys, to those of known Milky Way globular clusters. They find that $\sim 70\%$ of their sample of field stars have halo-like orbital properties, with only 20 stars having a

likely orbital association with an existing globular cluster. They do, however, claim that the orbital properties of halo stars seem to be compatible with the globular cluster escapee scenario. Similarly, Tang et al. (2020) compare the kinematics of ~ 100 N-rich stars in LAMOST DR5 to N-normal metal-poor field stars. They conclude that the orbital parameters of N-rich field stars indicate that most of them are inner-halo stars, and that the kinematics of these stars support a possible GC origin. Note that an alternative way to produce these N-rich stars has been proposed by Bekki (2019).

In this paper, we aim to constrain the origin of N-rich stars located in the Galactic bulge, on the basis of their chemo-dynamical properties. Identifying a population of accreted and *in situ* N-rich stars defined chemically, which are also confirmed by kinematics, we find that the ratio of N-rich to N-normal differ substantially between accreted and *in situ* populations.

This paper is organised as follows: In Section 2 we describe the data and the criteria for our sample. The results are presented and discussed in Section 3, and our conclusions are summarised in Section 4.

2 DATA & SAMPLE

The results in this paper are based on elemental abundances, radial velocities and stellar parameters from Data Release 16 of the APOGEE-2 survey (Majewski et al. 2017; Blanton et al. 2017; Ahumada et al. 2020) and proper motions from *Gaia*-DR2 (Gaia Collaboration et al. 2016, 2018). We make use of the publicly available code `galpy`² (Bovy 2015; Mackereth & Bovy 2018) to calculate orbital parameters adopting a McMillan (2017) potential. We also use distances from Leung & Bovy (2019b) which are generated using the `astroNN` python package (Leung & Bovy 2019a). The distances are determined using a training set that comprises APOGEE spectra and *Gaia*-DR2 parallax measurements for the purpose of predicting stellar luminosity from spectra. The model is able to simultaneously predict distances and accounts for the parallax offset present in *Gaia*-DR2, producing high precision, accurate distance estimates for APOGEE stars, which match well with external catalogues and standard candles.

2.1 APOGEE DR16

APOGEE-2, one of the four SDSS-IV (Blanton et al. 2017; Ahumada et al. 2020) experiments, has obtained near-infrared (NIR), high SNR ($S/N > 100 \text{ pixel}^{-1}$) and high resolution ($R \sim 22,500$) H-band spectra for more than 450,000 Milky Way stars, from which precision radial velocities, stellar parameters, and abundances for up to 26 elements are determined. APOGEE-2 uses two twin NIR spectrographs (Wilson et al. 2019) attached to the 2.5 m telescopes at Apache Point (Gunn et al. 2006), and Las Campanas Observatories (Bowen & Vaughan 1973). A more in-depth description of the APOGEE survey, target selection, raw data, data reduction and spectral analysis pipelines can be found in Majewski et al. (2017), Zasowski et al. (2017), Holtzman et al. (2015), Jönsson et al. (2018), Nidever et al. (2015), respectively (see Jönsson et al. (2020) for a complete up-to-date description of the latest APOGEE data released in DR16). The data are first reduced (Nidever et al. 2015 & Jönsson et al. 2020) using the APREAD and APSTAR pipelines, respectively. The data are then fed into the APOGEE Stellar Parameters

¹ To obtain these numbers, Schiavon et al. (2017) applied the Besançon models (Robin et al. 2012, 2014) in order to estimate the contribution of the inner stellar halo to the mass budget of the inner Galaxy.

² <http://github.com/jobovy/galpy>

and Chemical Abundance Pipeline (ASPCAP; García Pérez et al. 2016; Jönsson et al. 2020), which uses libraries of synthetic spectra (Zamora et al. 2015; Holtzman et al. 2018; and Jönsson et al. 2020) calculated using customised H -band line list (Shetrone et al. 2015); Smith et al. in prep, from which outputs are analysed, calibrated and tabulated (Holtzman et al. 2018; Jönsson et al. 2020).

2.2 Sample selection

We restrict our sample to stars that have $\text{ASPCAPFLAG} = 0$, $\text{SNR} > 70$ and distance uncertainty $< 20\%$ (i.e. $d_{\text{err}}/d < 0.2$). By performing these cuts, we obtain a reduced sample of APOGEE DR16 for which we can obtain reliable chemo-dynamic information. A further cut of $\log g < 3$ is also made to remove dwarf stars.

In addition, to ensure our sample is free from any stars residing in existing GCs, we remove from our sample any stars belonging to the GC member list from Horta et al. (2020). Furthermore, this paper focuses on stars in the Galactic bulge, so we make a spatial cut and select only stars with Galactocentric distance $R_{GC} < 4$ kpc. The effective temperature of these stars is further constrained to the range $3250 \text{ K} < T_{\text{eff}} < 4500 \text{ K}$. The lower T_{eff} limit is adopted to avoid very cool stars whose elemental abundances are affected by important systematic effects. The upper limit aims to eliminate from the sample C and N abundances that are uncertain due the weakness of CN and CO lines in spectra of warm stars with relatively low metallicity ($[\text{Fe}/\text{H}] < -1$). The bulge selection criteria can be summarised as:

- (i) $\text{ASPCAPFLAG} = 0$
- (ii) $R_{GC} < 4$ kpc
- (iii) $d_{\text{err}}/d < 0.2$
- (iv) $3250 \text{ K} < T_{\text{eff}} < 4500 \text{ K}$
- (v) $\log g < 3$
- (vi) $\text{SNR} > 70$

To select our sample of N-rich stars, we follow the sigma clipping methodology implemented in Schiavon et al. (2017). By inspecting the bulge stars in the $[\text{N}/\text{Fe}]$ - $[\text{Fe}/\text{H}]$ plane, N-rich stars are defined as those deviating by more than 5.5σ from a 4th order polynomial fit to the data in the bulge sample. The polynomial is given by:

$$[\text{N}/\text{Fe}] = 0.256 + 0.239 [\text{Fe}/\text{H}] - 0.072 [\text{Fe}/\text{H}]^2 - 0.304 [\text{Fe}/\text{H}]^3 - 0.091 [\text{Fe}/\text{H}]^4 \quad (1)$$

We further restrict these N-rich stars to those with $[\text{C}/\text{Fe}] < 0.15$, in order to limit our sample to stars which present the typical N-C anti-correlation of SG GC stars. Application of these selection criteria leaves us with a sample of 83 N-rich stars within the bulge sample of 14,448 stars.

In this paper we adopt a more stringent threshold of 5.5σ to define N-rich stars than the 4σ threshold adopted by Schiavon et al. (2017). In both cases, the threshold decision was informed by the distribution of N-rich stars in abundance planes such as those in Figure 4, where N-rich stars display (anti-)correlations between various abundance ratios. The threshold was chosen so as to clean the N-rich sample from contaminants due to abundance errors and statistical fluctuations. That philosophy is aimed at prioritising N-rich sample purity over completeness. That our threshold is more stringent than that adopted by Schiavon et al. (2017) reflects the fact that our parent sample is considerably larger, requiring a larger threshold to minimise contamination by outliers due to statistical fluctuations.

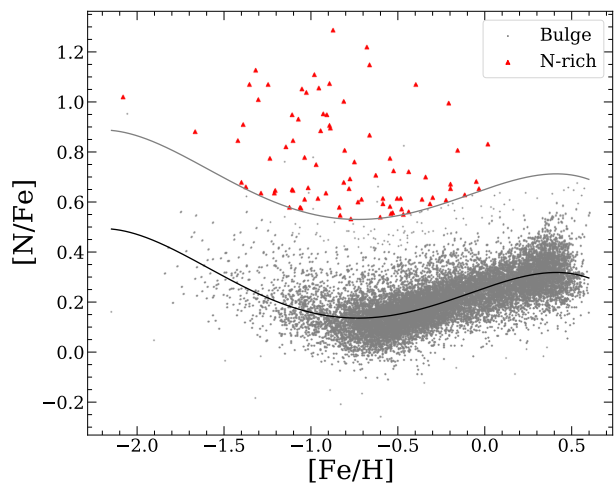


Figure 1. Distribution of sample stars in $[\text{N}/\text{Fe}]$ - $[\text{Fe}/\text{H}]$ plane. The small grey dots show the bulge population as selected in Section 2.2. The red triangles indicate the N-rich stars, defined as stars which deviate from the 4th order polynomial fit (black line) by more than 5.5σ and have $[\text{C}/\text{Fe}] < 0.15$.

We also look at the possible contamination to our sample of N-rich stars by AGB stars, which can also present an abundance pattern characterised by Nitrogen enrichment and Carbon depletion (Renzini & Voli 1981; Charbonnel & Lagarde 2010; Ventura et al. 2013). We identified 5 N-rich AGB candidates by their position on the $\log g - T_{\text{eff}}$ plane, hand picking those that have low $\log g$, high T_{eff} and relatively high $[\text{Fe}/\text{H}]$ compared to other stars in their neighbourhood, corresponding to $\sim 6\%$ of the sample, in agreement with theoretical expectations (Girardi et al. 2010). Due to the difficulty of individually selecting AGBs in our large sample of bulge field stars, we decide to keep the N-rich AGBs in our sample for consistency. We note that the results of this paper are largely unaffected by the presence of these N-rich AGBs.

3 RESULTS

In this section, we discuss how our sample of accreted and *in situ* populations are selected, employing methods used in Mackereth et al. (2019). We then discuss how these populations differ from each other in orbital space, and show the similarities of the N-rich stars to GC members in chemical space.

3.1 Selecting accreted and *in situ* stars

In order to split our sample into accreted and *in situ* groups, we study the distribution of stars in the α -Fe plane. Mackereth et al. (2019) achieved that by examining the distribution of their sample in the Mg-Fe plane, whereas Horta et al. (2021a) focused on the distribution in the $[\text{Mg}/\text{Mn}]$ vs $[\text{Al}/\text{Fe}]$ plane. We cannot proceed in the same way, because the abundances of Al and Mg are affected by the multiple populations phenomenon in GCs (e.g., Bastian & Lardo 2018; Mészáros et al. 2015, 2020), so that the positions of N-rich stars in chemical planes involving those elements cannot be interpreted in the same way as those of normal stars. Therefore, we use Si as the tracer of α -element abundances, because this element does not present substantial star-to-star variations in Galactic GCs.

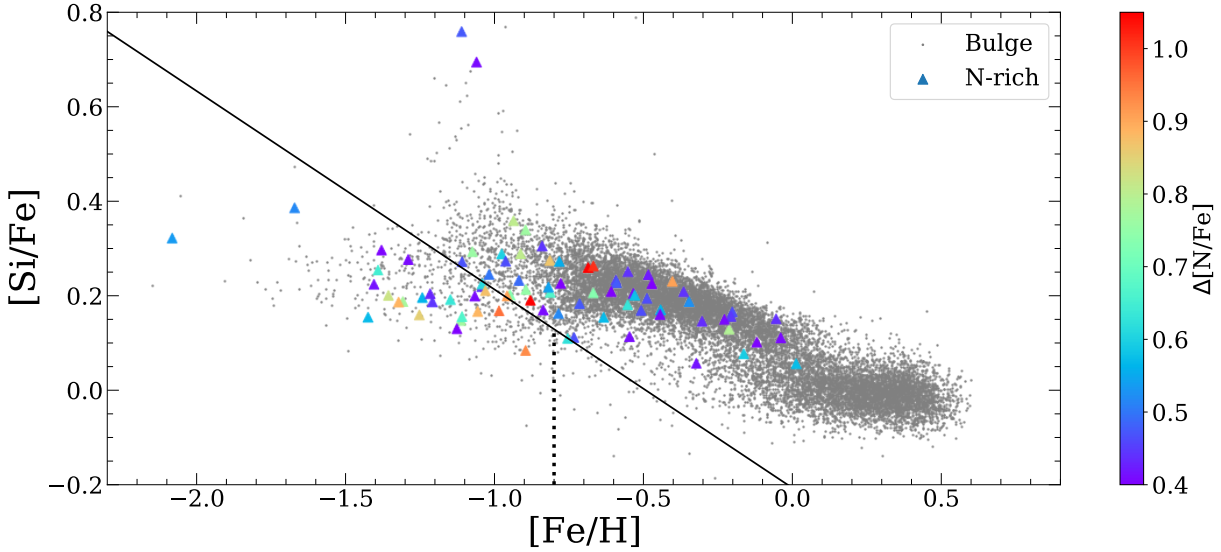


Figure 2. Distribution of sample stars in [Si/Fe]-[Fe/H] plane. The grey points show the distribution of the bulge stars, and the triangles, coloured according to the [N/Fe] residuals of the polynomial fit shown in Figure 1, show the N-rich stars distribution in this plane. The solid black line is the cut made to separate the accreted stars from the *in situ* stars shown in Mackereth et al. (2019), adjusted to account for the metallicity gradient of disk populations between the outer and inner halo. The cut of [Fe/H] < -0.8 to remove disk contaminants is shown as the vertical dotted line.

The data in Figure 2 show that the N-rich star population occupies the same locus in the Si-Fe plane as the overall bulge field population. Following Mackereth et al. (2019), we split the sample between accreted and *in situ* populations. To determine where the dividing line is drawn in the [Si/Fe] vs [Fe/H] plane, we proceed as follows: 1) Following Mackereth et al. (2019), we choose a slope that approximately matches the mean slope of the high- and low- α populations, slightly adjusting it to minimise the contamination of the accreted populations by low- α disk stars; 2) We calculate the distance in [Fe/H] between the dividing line and the mean value of the low-Mg disk population and adjust the zero-point so that the distance is the same in the [Si/Fe] vs [Fe/H] plane; 3) We further shift the zero-point by +0.2 dex in [Fe/H], to account for the disk metallicity gradient (e.g., Hayden et al. 2015). The resulting linear relation is given by:

$$[\text{Si}/\text{Fe}] = -0.42 ([\text{Fe}/\text{H}] + 0.016) + 0.2 \quad (2)$$

Because this relation may be considered somewhat arbitrary, we estimate how a ± 0.1 dex zero-point variation impacts our results (see discussion in Section 3.3)

We make a further cut in metallicity to the accreted population of [Fe/H] < -0.8, to minimise contamination from disk stars. This latter cut removes 38 bulge stars from our accreted population, bringing the total number of bulge stars down to 14,410. We henceforth refer to stars below (above) and to the left (right) of the dividing line as "accreted" (*in situ*) populations. The resulting accreted and *in situ* general bulge samples comprise 428 and 13,982 stars, respectively, with 25 N-rich stars being located in the accreted locus, and 58 located in the *in situ* region. Thus, we conclude that roughly $\sim 30\%$ of the N-rich stars in the inner Galaxy have an accreted origin. We emphasise here that stars in each sub-sample are found across the entire inner Galaxy.

Figure 3 shows where these sub-samples lie in the [Al/Fe]-[N/Fe] plane. By placing stars in this plane, former GC members can be identified as those that follow a positive correlation between

those two abundance ratios. When displaying our sample on this plane, we can see that the accreted and *in situ* bulge populations occupy slightly different loci. While N and Al abundances of N-rich stars are correlated in both *in situ* and accreted sub-samples, the correlations in each sub-sample are slightly different. The [Al/Fe] ratios of N-normal stars in the accreted sample, save for a handful of outliers, are lower than those in their *in situ* counterparts, on average by ~ 0.2 dex. This result validates our definition of accreted vs *in situ* populations, since the accreted stars with first-generation-like abundance patterns (i.e., those not affected by multiple population effects) are consistent with a dwarf galaxy origin (e.g., Mackereth et al. 2019; Helmi 2020; Das et al. 2020; Horta et al. 2021a).

We identify a group of Si-rich stars, with [Si/Fe] $\geq +0.5$ in the metallicity range $-1.3 < [\text{Fe}/\text{H}] < -0.9$. They are similar to those spotted by Masseron et al. (2019) within the MW GCs M92, M15 and M13. Those authors showed that, in the most metal-poor GCs, M92 and M15, Si-rich stars are characterised by very low [Mg/Fe], whereas stars in M13 had normal [Mg/Fe]. The Si-rich stars in our sample have normal [Mg/Fe], resembling those Masseron et al. (2019) identified in M13. We ascribe a GC origin to these field Si-rich stars and discuss their kinematic properties in Section 3.3.

3.2 Comparison with GCs

To confirm the association of the field N-rich stars with GCs, we overplot our sample of N-rich stars on data for GC members from Horta et al. (2020) in three different chemical planes. We show the correlations of GC stars in Mg-Al, Al-N and N-C space. In each panel the N-rich stars lie on the same locus as SG GC stars, which supports our assumption that they are, in fact, former GC members. For clarity, the accreted and *in situ* populations are plotted on different panels of Figure 4 because they span different metallicity regimes. Abundances of field stars in each set of panels are compared with those of members of GCs whose mean chemical

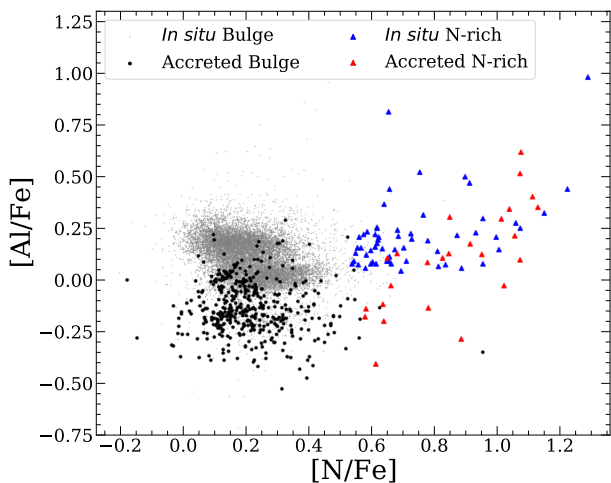


Figure 3. Distribution of *in situ* bulge (small grey dots), accreted bulge (black dots), *in situ* N-rich (blue triangles) and accreted N-rich (red triangles) stars in [Al/Fe]-[N/Fe] plane. The N-rich stars show a correlation between [N/Fe] and [Al/Fe], which is also observed in SG GC stars. However, the correlations are slightly different between the accreted and *in situ* populations. The accreted bulge stars are seen to occupy a lower locus in [Al/Fe] than the *in situ* by ~ 0.2 dex, which is consistent with a dwarf galaxy origin.

compositions locate them in the accreted and *in situ* loci of the Si-Fe plane. For the comparison with accreted N-rich stars we select NGC5904 (258 stars, $\langle[\text{Fe}/\text{H}]\rangle = -1.14$, $\langle[\text{Si}/\text{Fe}]\rangle = 0.18$) and NGC6205 (119 stars, $\langle[\text{Fe}/\text{H}]\rangle = -1.44$, $\langle[\text{Si}/\text{Fe}]\rangle = 0.19$), and for the *in situ* N-rich stars we select NGC6553 (52 stars, $\langle[\text{Fe}/\text{H}]\rangle = -0.04$, $\langle[\text{Si}/\text{Fe}]\rangle = 0.06$) and NGC104 (333 stars, $\langle[\text{Fe}/\text{H}]\rangle = -0.67$, $\langle[\text{Si}/\text{Fe}]\rangle = 0.21$)

On the plots in the first row, the anti-correlation between Al and Mg appears to differ substantially between the metal-poor and metal-rich sub-samples of GCs. The metal-rich GC sub-sample shows a smaller scatter in both [Al/Fe] and [Mg/Fe] than those shown by the metal-poor sub-sample. Therefore, while the anti-correlation is easily visible in the metal-poor sample, it is not evident in the metal-rich sample. This is similarly shown in the Al-N plots. Where, though the correlation can be seen in the metal-rich GCs, it is more easily identified in the metal-poor GC sub-sample. For a more detailed discussion, see Mészáros et al. (2015) and Nataf et al. (2019).

In a recent paper, Fernández-Trincado et al. (2019) claim that N-rich stars must have $[\text{Al}/\text{Fe}] > +0.5$ to be considered SG GC members. Application of that criterion would remove large numbers of N-rich stars from our sample. However, we argue that our sample of field N-rich are indeed akin to SG GC members for the following reason: the bottom panels of Figure 4 show a clear bimodality in the [N/Fe]-[C/Fe] plane, with the SG GC stars located and higher [N/Fe] above their FG GC counterparts. The dividing line between the two populations is located roughly at $[\text{N}/\text{Fe}] = +0.5$ for $[\text{C}/\text{Fe}] = -0.5$, and gently decreasing [N/Fe] for increasing [C/Fe]. This bimodality is also present in both the [Al/Fe]-[Mg/Fe] and [Al/Fe]-[N/Fe], showing that there are SG GC stars with $[\text{Al}/\text{Fe}] < 0.5$ all the way to below solar. In fact, application of an $[\text{Al}/\text{Fe}] > +0.5$ cut would remove a large fraction of the SG stars in GCs themselves, particularly in the low metallicity regime (left panels of Figure 4). It is also well known that, although SG GCs typically present enhancements in N, Al and Na (Bastian & Lardo 2018), not all stars in GCs that

are enhanced in N are also enhanced in Al. Indeed, as mentioned above, the Al-Mg anti-correlation is dependent on metallicity, being substantially weaker in metal-rich GCs (e.g., Mészáros et al. 2015; Nataf et al. 2019; Mészáros et al. 2020), and mass (Massari et al. 2017).

3.3 Kinematic properties

In this sub-section we check whether our definition of accreted and *in situ* stars, which is based solely on chemistry, maps into distinct properties in kinematic space. To do this, we make comparisons between the distributions of our samples in a kinematic diagram, which is used to distinguish components of the Galaxy on the basis of their kinematic signatures (e.g., Venn et al. 2004; Bonaca et al. 2017; Helmi et al. 2018; Koppelman et al. 2019). The x-axis of the kinematic diagram is the tangential velocity, v_ϕ , while the y-axis is the quadrature sum of the radial and vertical velocities, $\sqrt{v_R^2 + v_Z^2}$.

The accreted and *in situ* populations are displayed on the kinematic diagram separately on the upper and lower panels of Figure 5, respectively. Since the velocities are in Galactocentric coordinates, this places the origin of the coordinate system at the Galactic Centre, therefore the velocity of the Sun is at $v_{LSR} \sim 220$ km/s. In both panels normal stars are displayed as black/gray dots and N-rich stars as coloured triangles. Visual examination of these plots suggests the following interesting trend: Accreted stars, both normal and N-rich, have on average more retrograde orbits ($v_\phi < 0$) than their *in situ* counterparts, whose orbits are predominantly prograde. This is clearly shown by the difference in the v_ϕ distribution of the *in situ* and accreted samples of N-rich stars, with the mean of the latter being ~ 80 km/s lower than that of the former.

The above visual impressions must be confirmed by a quantitative statistical evaluation. The Kolmogorov-Smirnov (KS) statistic is a nonparametric test used to assess the similarity between two samples. We use the python package `ndtest`³ to make 2D comparisons between the distributions in v_ϕ and $\sqrt{v_R^2 + v_Z^2}$ of the following sub-samples, as shown in Table 1: accreted N-rich vs. accreted normal, *in situ* N-rich vs. *in situ* normal, accreted N-rich vs. *in situ* N-rich and, accreted normal vs. *in situ* normal. The KS tests result in a rejection of the null hypothesis, with p -value < 0.1 for all four comparisons. The clear kinematic distinction between the accreted and *in situ* populations confirms our chemical selection of these groups. We also note the difference between accreted N-rich vs. accreted normal sub-samples. This result can be understood by examination of Figure 6. In that plot it can be seen that the accreted normal stars show a clump of slightly prograde stars around $E/10^5 \sim -2.2$ km²s⁻², without a clear counterpart in the N-rich accreted group. We suspect that this prograde population is likely due to contamination from the disk. In addition, the accreted normal population hosts a number of stars forming a cloud with $E/10^5 \gtrsim -1.85$ km²s⁻², where no N-rich stars can be found. That is the locus occupied by stars belonging to the GE/S system, as well as other possible accretion events (Ibata et al. 1994; Helmi et al. 1999; Ibata et al. 2016; Belokurov et al. 2018; Haywood et al. 2018; Helmi et al. 2018; Mackereth et al. 2019; Horta et al. 2021a). Conversely, most of the N-rich stars occupy the same locus as Heracles identified recently by Horta et al. (2021a), with a couple of stars displaying kinematics suggestive of disk-like orbits.

Interestingly, the KS test rejects the null hypothesis for similarity between the *in situ* N-rich vs. *in situ* normal sub-samples. We

³ <https://github.com/syrte/ndtest>

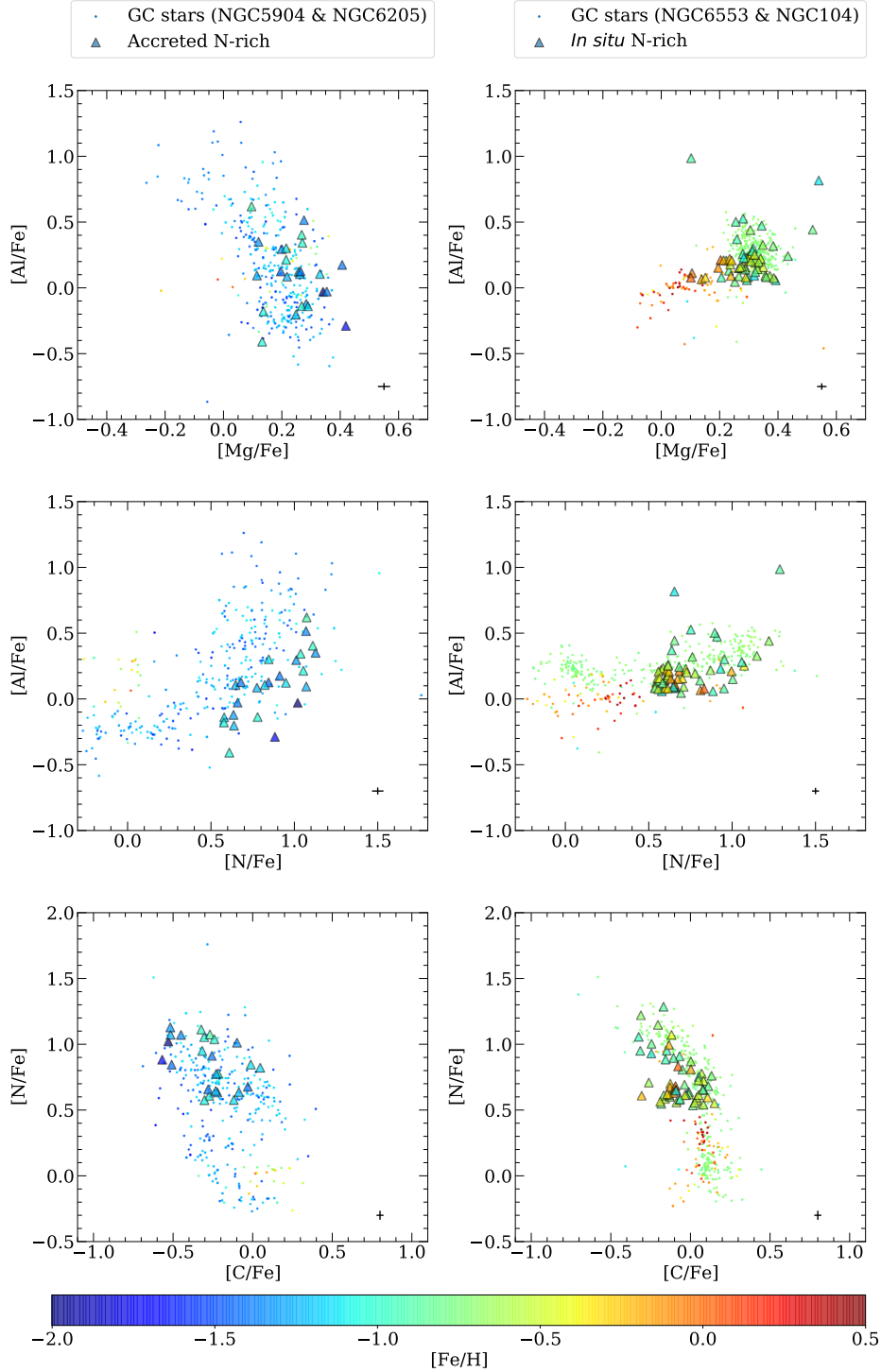


Figure 4. Coloured dots and triangles indicate GC stars (Horta et al. 2020) and N-rich stars (see Section 2.2), respectively, colour coded by their [Fe/H] abundance. The graphs on the left show the accreted N-rich stars plotted on top of stars in NGC5904 and NGC6205, and the right graphs show the *in situ* N-rich stars plotted on top of stars in NGC6553 and NGC104, both using the same metallicity colour scale. Each plot shows the mean errorbar for the N-rich stars in the bottom right corner. The 1st row shows these stars in the [Al/Fe]-[Mg/Fe] plane to show the Al-Mg anti-correlation in GCs. The 2nd row shows the distribution in the [Al/Fe]-[N/Fe] plane to show the Al-N correlation in GCs. The 3rd row shows the distribution in the [N/Fe]-[C/Fe] plane to show the N-C anti-correlation in GCs. Each plot shows that our sample of N-rich stars lies on the same locus as SG GC members, supporting the idea they have possible GC origin.

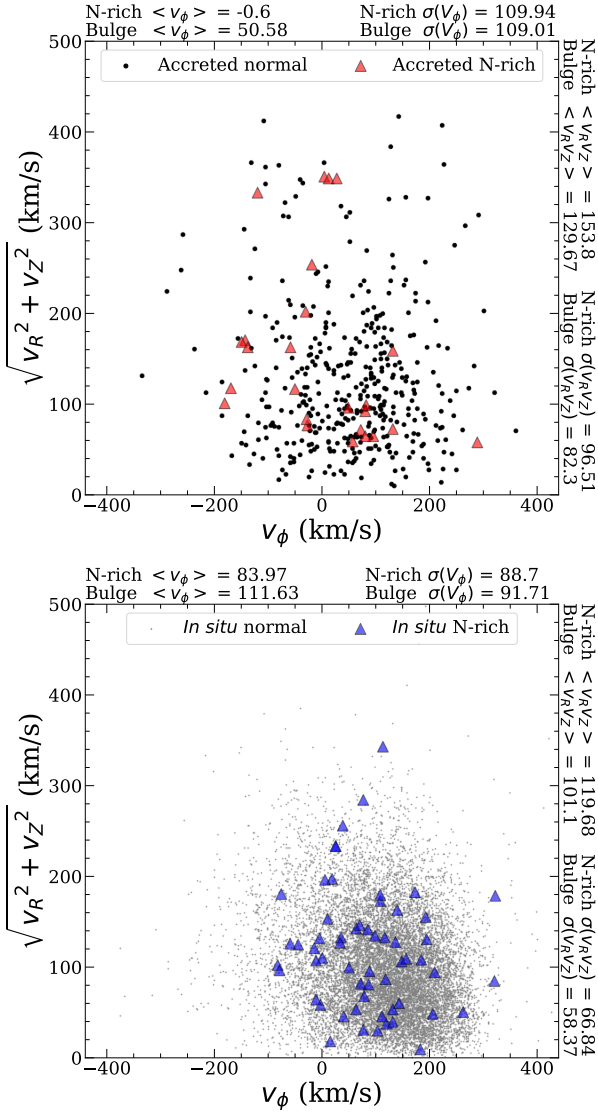


Figure 5. Distribution in $\sqrt{v_R^2 + v_Z^2}$ vs. v_ϕ of accreted and *in situ* stars on the top and bottom panel respectively. *Top Panel:* Accreted N-rich stars (red triangles) and the accreted bulge stars (black dots). *Bottom Panel:* *in situ* N-rich stars (blue triangles) and *in situ* bulge stars (grey dots). Anything with $v_\phi > 0$ has a prograde orbit, similar to that of the disk, and anything with $v_\phi < 0$ has a retrograde orbit. We also show on these plots the mean and standard deviation of the sub-samples for each axis.

suggest that the difference between these two sub-samples is due to the presence of disk stars within 4 kpc of the Galactic centre. This is further discussed in Section 3.4

The stars in the accreted sample have on average lower metallicities than their *in situ* counterparts. Thus, the differences encountered could be due to the dependence of kinematics on the metallicity of stellar populations. To test that hypothesis, we redo the KS tests to assess the similarity between the accreted and *in situ* sub-samples, this time limiting the comparison to stars with $[\text{Fe}/\text{H}] < -0.8$. The results from this comparison are shown in Table 1. The difference between the N-rich and normal accreted populations remain unchanged since they were already restricted to $[\text{Fe}/\text{H}] < -0.8$. We do, however, see a big change in the com-

Comparison	<i>p</i> -value
Accreted N-rich vs. Accreted normal	0.024
<i>In situ</i> N-rich vs. <i>In situ</i> normal	0.028
Accreted normal vs. <i>In situ</i> normal	< 0.001
Accreted N-rich vs. <i>In situ</i> N-rich	0.009
Comparison ($[\text{Fe}/\text{H}] < -0.8$)	
Accreted N-rich vs. Accreted normal	0.024
<i>In situ</i> N-rich vs. <i>In situ</i> normal	0.294
Accreted normal vs. <i>In situ</i> normal	0.038
Accreted N-rich vs. <i>In situ</i> N-rich	0.027
Comparison (Zero-point +0.1 dex)	
Accreted N-rich vs. Accreted normal	0.066
<i>In situ</i> N-rich vs. <i>In situ</i> normal	0.062
Accreted normal vs. <i>In situ</i> normal	< 0.001
Accreted N-rich vs. <i>In situ</i> N-rich	0.040
Comparison (Zero-point -0.1 dex)	
Accreted N-rich vs. Accreted normal	0.172
<i>In situ</i> N-rich vs. <i>In situ</i> normal	0.006
Accreted normal vs. <i>In situ</i> normal	< 0.001
Accreted N-rich vs. <i>In situ</i> N-rich	0.223

Table 1. Results obtained from performing a 2D KS test between the different sub-samples shown in Figure 5. *First Panel:* *p*-values for the comparisons between sub-samples as defined in Section 3.1. *Second Panel:* *p*-values for the comparisons between the sub-samples with $[\text{Fe}/\text{H}] < -0.8$. *Third & Fourth Panel:* Result when shifting the zero-point of the dividing line, Equation 2, by ± 0.1 dex. Setting a threshold for the *p*-value of 0.1. So, a *p*-value < 0.1 results in a rejection of the null hypothesis, whereas a *p*-value > 0.1 means the null hypothesis cannot be rejected.

parison between the *in situ* populations, where the *p*-value = 0.294 tells us that the null hypothesis cannot be rejected. This is due to the removal of high metallicity disk stars from our sample of *in situ* normal stars. Regarding the comparison between accreted and *in situ* populations, for both the N-rich and normal samples, the null hypothesis is rejected even when the comparison is limited to metal-poor sub-samples. In short, accreted and *in situ* samples are kinematically different populations even when only metal-poor stars are considered.

We checked whether our results are sensitive to the definition of the line separating accreted and *in situ* populations in Figure 2. For that purpose, we shifted the zero-point of the relation given by the Equation 2 by ± 0.1 dex in $[\text{Fe}/\text{H}]$, the results for which are shown in the bottom two panels of Table 1. When increasing the zero-point by +0.1 dex, our results are unchanged. However, when shifting the relation towards lower $[\text{Fe}/\text{H}]$, the KS tests become consistent with the null hypothesis for two of the sub-sample comparisons: (i) accreted normal vs. accreted N-rich stars. This result is due to the removal of a small number of retrograde N-rich stars and the reduction in the contribution of prograde normal stars (which we conjectured in Section 3.3 to be due to disk contamination); (ii) accreted N-rich vs. *in situ* N-rich stars. This happens because the above mentioned retrograde N-rich stars that are moved from the accreted to the *in situ* sub-sample, make the two groups more similar kinematically. Since this exercise leads to a reduction of the size of the N-rich accreted population, we deem these result of little statistical significance. The matter will have to be revisited on the basis of larger samples.

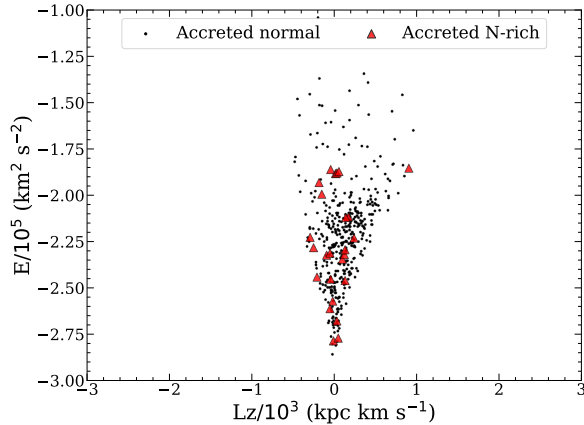


Figure 6. Accreted N-normal (black dots) shows a population of stars in the same locus as GE/S stars at high energies, whilst the accreted N-rich stars (red triangles) occupy the low energy region similar to Heracles.

Again, we check the dependence of kinematics on metallicity by limiting the comparison to stars with $[\text{Fe}/\text{H}] < -0.8$, as done above, after shifting the relation by ± 0.1 dex. The results for this are not shown since the only change we find is when comparing *in situ* N-rich and *in situ* normal sub-samples. In both cases, when moving the zero-point towards higher or lower $[\text{Fe}/\text{H}]$, the null hypothesis cannot be rejected when comparing these two sub-samples. Also in this case the statistical significance of the results is small due to the reduced sample sizes.

Finally, we examine the kinematic properties of Si-rich stars mentioned in Section 3.1 separately. When comparing their properties to those of N-rich and N-normal, the KS tests only yielded a statistically significant difference with the accreted N-rich, $p\text{-value}=0.022$. This suggests that this population is likely to result from the dissolution of *in situ* GCs and in the remainder of this analysis they will be treated as such.

In summary, the results above show that the chemistry-based definition of accreted and *in situ* sub-samples maps into distinct kinematic properties. Both N-rich and N-normal *in situ* samples with $R_{\text{GC}} < 4$ kpc show more disk-like orbits than their accreted counterparts, according to expectations. In Horta et al. (2021a) we showed that there is an important contamination of the chemically defined accreted samples by *in situ* stars. However, the differences persist even when controlling for the dependence of kinematics on metallicity, which argues in favour of our interpretation of the origin of the accreted N-rich sample.

3.4 N-rich stars frequency in accreted and *in situ* samples

An important clue to the origin of N-rich stars is their frequency, f_{N_r} , defined as the ratio between the number of such stars and the total field population (e.g., Martell et al. 2016; Schiavon et al. 2017; Koch et al. 2019; Horta et al. 2021b). We measured this frequency in both the accreted and *in situ* sub-samples, and henceforth express it in terms of percentages. In the accreted group we find $f_{N_r} = 5.84 \pm 1.28\%$, whereas for the *in situ* group, the measured frequency is an order of magnitude lower, $f_{N_r} = 0.41 \pm 0.05\%$, $f_{N_r} = 0.60 \pm 0.08\%$ if only high- α stars are considered. If we account for the Si-rich stars identified in Section 3.1, ascribing them to an *in situ* GC origin based

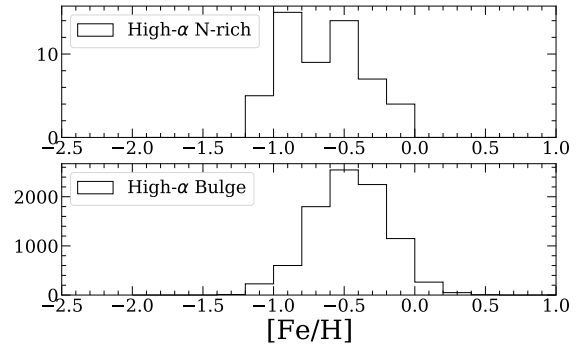


Figure 7. Metallicity distribution functions (MDFs) for the *in situ* high- α N-rich stars (top panel) and *in situ* high- α normal field (bottom panel). The MDFs of the two populations are not very different. The N-rich MDF peaks at a slightly lower $[\text{Fe}/\text{H}]$, but is substantially broader, overlapping the high metallicity end of the N-normal MDF.

on their kinematics, the frequency of the *in situ* group increases to $f_{N_r} = 0.58 \pm 0.06\%$, $f_{N_r} = 0.86 \pm 0.10\%$ if only high- α stars are considered. Thus, consideration of Si-rich stars does not alter our finding of a large difference between accreted and *in situ* N-rich stars.

This difference cannot be easily understood. According to the prevailing scenario for GC formation and destruction, (Kruijssen 2014, 2015; Pfeffer et al. 2019) Galactic GCs originate from two different channels. The *ex situ*, or accreted, channel would consist of GCs that were accreted to the Galaxy along with their host galaxies. Those accretion episodes occurred predominantly, though not exclusively, in the early stages of the Milky Way assembly, as suggested by various lines of evidence (e.g., Deason et al. 2014; Mackereth et al. 2018, 2019; Pfeffer et al. 2019; Schiavon et al. 2020; Hughes et al. 2020). Conversely, the *in situ* population would be comprised of GCs that were formed in the turbulent disk of the Milky Way at $z \sim 2 - 3$. According to this scenario, *in situ* GCs would have been destroyed very efficiently by tidal interaction with giant molecular clouds in the early disk (the so-called “cruel cradle effect”, see Kruijssen et al. 2012), whereas destruction of accreted GCs via tidal stripping and evaporation was less efficient, having happened on a much longer timescale. Given these predictions, we would naively expect the frequency of *in situ* N-rich stars to be higher, not lower than that of the accreted population.

One possible way out of this conundrum is to invoke that the ratio between integrated star formation in the form of GCs over total was lower in the *in situ* than in the accreted population. This could be achieved, for instance, if the *in situ* population underwent a longer star formation episode than that leading up to the formation of the accreted population. If *in situ* star formation was extended further in time, after the cessation of the main episode of GC formation/destruction, a low *in situ* f_{N_r} could possibly be accommodated. In such a situation, however, one would expect the metallicity distribution function (MDF) of the *in situ* normal population to have more power towards higher metallicities than that of the *in situ* N-rich population.

This qualitative prediction does not seem to be supported by the metallicity distribution functions (MDFs) of the N-rich and N-normal bulge *in situ* samples, shown in Figure 7. For simplicity, we limit our comparison to high- α N-rich and normal field stars, as those are understood to have undergone a coherent chemical evolu-

tion path that is independent of the low- α disk population (Mackereth et al. 2018). In that figure, one can see that the MDFs of the high- α N-rich and N-normal *in situ* samples are not very different. The MDF of the high- α N-rich population peaks at $[\text{Fe}/\text{H}] \sim -0.8$, whereas that of the high- α N-normal population peaks at a slightly higher metallicity, around $[\text{Fe}/\text{H}] \sim -0.5$. That difference in the mode of the two MDFs is slightly offset by the fact that the N-rich population has a broader MDF, with $\text{FWHM} \sim 0.9$ dex, whereas that of the *in situ* population has $\text{FWHM} \sim 0.6$ dex. Assuming the N-rich MDF reproduces that of the parent GCs, one would thus conclude that the star formation history associated with the N-normal population did not extend in time much further past the period of GC formation and destruction. This result is additionally corroborated by recent evidence for a very fast overall formation of both the high- and low- α stellar populations in the inner Galaxy, which is attested by their predominantly old ages (e.g., Hasselquist et al. 2020).

This result prompts interesting considerations on the origin of the accreted N-rich stars currently inhabiting the inner Galaxy. The frequency of metal-poor N-rich stars as a function of Galactocentric distance has been shown by Horta et al. (2021b) to undergo a steep decrease towards growing R_{GC} (see also Martell et al. 2016; Koch et al. 2019). At $R_{\text{GC}} \sim 15$ kpc, Horta et al. (2021b) found $f_{N_r} \sim 3^{+1}_{-0.8}\%$, which is considerably lower than the ratio we find for the accreted population. Since the population of N-rich stars in our sample at low metallicity is dominated by accreted stars, this result leads to the conclusion that GC destruction associated with satellite mergers must have been very efficient in the early stages of the Galaxy’s formation. Indeed it has been shown by Pfeffer et al. (2020) that GCs associated with the earliest accretion events ended up in strongly bound orbits, driven by dynamical friction. That is the case for Heracles (Horta et al. 2021a), a $\sim 5 \times 10^8 M_{\odot}$ satellite that likely merged with the MW over 10 Gyr ago (see also Kruijssen et al. 2020). Given the coincidence between the positions of our bulge N-rich stars in integrals of motion space and those of Heracles stars (Figure 6), we speculate that the bulge N-rich population is partly made of members of GCs that were originally associated with Heracles, and were mostly destroyed during the accretion event. It is also possible that those accreted N-rich stars were already in the field of Heracles, before they were accreted to the MW, however there currently is no evidence for the presence of N-rich stars in the fields of dwarf satellites of the MW.

Hughes et al. (2020) used the E-MOSAICS simulations (Pfeffer et al. 2019) to calculate the contribution of destroyed GCs to field populations in the bulges of MW-like galaxies, comparing the predictions with the measurements by Schiavon et al. (2017). They show that, for most of the MW-like galaxies in their simulated volume, the prediction for f_{N_r} of the *metal-poor* stellar population is lower than the observations by factors of ~ 2 – 30 (bottom panel of their Figure 4). However, for a few simulated galaxies the predicted f_{N_r} are in good agreement with the observations. Like the MW, the disk populations of those galaxies are characterised by a bimodal distribution in the α -Fe plane, which is a distinctive feature of the MW disk populations (e.g., Hayden et al. 2015; Mackereth et al. 2017). Mackereth et al. (2018) showed that this feature is associated with an atypical accretion history, characterised by intense merging in early times and relative calm since $z \sim 1 - 1.5$. It is noteworthy, however, that Hughes et al. (2020) predictions for these few MW-like galaxies differ from our measurements with regards to the dependence of f_{N_r} on position in the α -Fe plane. The high frequency of ex-GC stars in the field of simulated galaxies is predominantly due to high- α *in situ* GC formation and destruction, whereas our data show that the high f_{N_r} in the MW bulge is due to the contribution

by the dissolution of low- α accreted GCs. This discrepancy would be alleviated if some of the stars in the accreted region in Figure 2 were in fact formed *in situ*, (see Figure 2 of Hughes et al. 2020), but it is not clear that accounting for such a contamination would completely eliminate the disagreement.

4 SUMMARY

The results presented in this paper make use of elemental abundances from APOGEE DR16 along with data from *Gaia* DR2 to study the chemical and kinematic properties of 146 N-rich stars located within the inner 4 kpc of the Galaxy. Our conclusions can be summarised as follows:

- We find that there are likely accreted and *in situ* components to the N-rich population within 4 kpc of the Galactic centre, identified via chemistry by making a cut in $[\alpha/\text{Fe}]-[\text{Fe}/\text{H}]$ space towards low metallicities (as shown in Figure 2) (e.g. Hayes et al. 2018; Mackereth et al. 2019; Das et al. 2020). By making this cut and removing stars without proper motions in *Gaia*, we select 428 and 13,982 bulge stars that lie in the accreted and *in situ* positions, respectively, with 25 N-rich stars being located in the accreted, and 58 located in the *in situ* locus.
- We show that our sample of N-rich stars occupies the same locus as so-called second-generation GC stars, supporting the idea that they are the by-products of GCs destruction/evaporation.
- We find that there is a significant difference in the kinematic properties of chemically defined accreted and *in situ* populations. This shows that our chemistry-based distinction of these populations maps into differences in kinematic space. We also find that the accreted bulge field population includes stars which share orbital properties with the GE/S system, although no N-rich stars occupy that locus of orbital parameter space. The absence of N-rich stars associated with GE/S in the bulge is likely due to their low frequency, combined with the relatively small number of GE/S stars found in the bulge (see Horta et al. 2021a)
- We find that the frequency of N-rich stars differs by an order of magnitude between the accreted ($f_{N_r} = 5.84 \pm 1.28\%$) and *in situ* ($f_{N_r} = 0.41 \pm 0.05\%$) samples. This result seems to be at odds with numerical simulations that predict a higher frequency of destroyed GCs among high- α *in situ* populations (Hughes et al. 2020). We speculate that the higher frequency of N-rich stars among accreted populations is due to early merger events, such as Heracles (Horta et al. 2021a), which likely had their GCs destroyed very efficiently during the merger with the MW.
- The identification of an accreted population of N-rich stars in the bulge raises the question of whether the GCs from which they originate were destroyed in their host dwarf galaxies or during the merger. If the former hypothesis is correct, we would expect that N-rich stars would be present in the field of current Milky Way satellites. Norris et al. (2017) did not find a Na-O anti-correlation, which is typical of GC stars, in Carina dwarf spheroidal field stars. However, their study is based on a sample of 63 stars, which is relatively small. Since the observed frequency of N-rich stars in the halo is $\sim 3\%$ one would expect to find ~ 2 N-rich stars in the sample of Norris et al. (2017). Such low numbers could easily be missed due to stochastic sampling.

ACKNOWLEDGEMENTS

We thank all those professionals who have been working tirelessly during these difficult times so that people like ourselves can work safely from home. The authors thank Nate Bastian and Meghan Hughes for helpful discussion. SSK acknowledges an STFC doctoral studentship. The anonymous referee is thanked for an insightful review of the original manuscript. JTM acknowledges support from the ERC Consolidator Grant funding scheme (project ASTEROCHRONOMETRY, <https://www.asterochronometry.eu>, G.A. n. 772293). S.H. is supported by an NSF Astronomy and Astrophysics Postdoctoral Fellowship under award AST-1801940. DAGH acknowledges support from the State Research Agency (AEI) of the Spanish Ministry of Science, Innovation and Universities (MCIU) and the European Regional Development Fund (FEDER) under grant AYA2017-88254-P.

Funding for the Sloan Digital Sky Survey IV has been provided by the Alfred P. Sloan Foundation, the U.S. Department of Energy Office of Science, and the Participating Institutions. SDSS acknowledges support and resources from the Center for High-Performance Computing at the University of Utah. The SDSS web site is www.sdss.org.

SDSS is managed by the Astrophysical Research Consortium for the Participating Institutions of the SDSS Collaboration including the Brazilian Participation Group, the Carnegie Institution for Science, Carnegie Mellon University, the Chilean Participation Group, the French Participation Group, Harvard-Smithsonian Center for Astrophysics, Instituto de Astrofísica de Canarias, The Johns Hopkins University, Kavli Institute for the Physics and Mathematics of the Universe (IPMU) / University of Tokyo, the Korean Participation Group, Lawrence Berkeley National Laboratory, Leibniz Institut für Astrophysik Potsdam (AIP), Max-Planck-Institut für Astronomie (MPIA Heidelberg), Max-Planck-Institut für Astrophysik (MPA Garching), Max-Planck-Institut für Extraterrestrische Physik (MPE), National Astronomical Observatories of China, New Mexico State University, New York University, University of Notre Dame, Observatório Nacional / MCTI, The Ohio State University, Pennsylvania State University, Shanghai Astronomical Observatory, United Kingdom Participation Group, Universidad Nacional Autónoma de México, University of Arizona, University of Colorado Boulder, University of Oxford, University of Portsmouth, University of Utah, University of Virginia, University of Washington, University of Wisconsin, Vanderbilt University, and Yale University.

DATA AVAILABILITY

Most of the data upon which this paper is based are publicly available as part of the 16th data release of the Sloan Digital Sky Survey (SDSS-IV) collaboration. For part of the sample, the data are still proprietary and will be made publicly available as part of the 17th data release. Once the latter data are publicly available they will be accessible via the usual channels.

REFERENCES

Ahumada R., et al., 2020, *ApJS*, 249, 3
 Bastian N., Lardo C., 2018, *ARA&A*, 56, 83
 Bekki K., 2019, *MNRAS*, 490, 4007
 Belokurov V., Erkal D., Evans N. W., Koposov S. E., Deason A. J., 2018, *MNRAS*, 478, 611

Blanton M. R., et al., 2017, *AJ*, 154, 28
 Bonaca A., Conroy C., Wetzel A., Hopkins P. F., Kereš D., 2017, *ApJ*, 845, 101
 Bovy J., 2015, *ApJS*, 216, 29
 Bowen I. S., Vaughan A. H. J., 1973, *Appl. Opt.*, 12, 1430
 Carollo D., Martell S. L., Beers T. C., Freeman K. C., 2013, *ApJ*, 769, 87
 Charbonnel C., Lagarde N., 2010, *A&A*, 522, A10
 Das P., Hawkins K., Jofré P., 2020, *MNRAS*,
 Deason A. J., Belokurov V., Koposov S. E., Rockosi C. M., 2014, *ApJ*, 787, 30
 Elmegreen B. G., 2010, *ApJ*, 712, L184
 Fernández-Trincado J. G., Beers T. C., Tang B., Moreno E., Pérez-Villegas A., Ortigoza-Urdaneta M., 2019, *MNRAS*, 488, 2864
 Gaia Collaboration et al., 2016, *A&A*, 595, A1
 Gaia Collaboration et al., 2018, *A&A*, 616, A1
 García Pérez A. E., et al., 2016, *AJ*, 151, 144
 Girardi L., et al., 2010, *ApJ*, 724, 1030
 Gnedin O. Y., 2001, *Astronomical and Astrophysical Transactions*, 20, 39
 Gunn J. E., et al., 2006, *AJ*, 131, 2332
 Hanke M., Koch A., Prudil Z., Grebel E. K., Bastian U., 2020, *A&A*, 637, A98
 Hasselquist S., et al., 2020, *ApJ*, 901, 109
 Hayden M. R., et al., 2015, *ApJ*, 808, 132
 Hayes C. R., et al., 2018, *ApJ*, 852, 49
 Haywood M., DiMatteo P., Lehnert M. D., Snaith O., Khoperskov S., Gómez A., 2018, *ApJ*, 863, 113
 Helmi A., 2020, *ARA&A*, 58, 205
 Helmi A., White S. D. M., de Zeeuw P. T., Zhao H., 1999, *Nature*, 402, 53
 Helmi A., Babusiaux C., Koppelman H. H., Massari D., Veljanoski J., Brown A. G. A., 2018, *Nature*, 563, 85
 Holtzman J. A., et al., 2015, *AJ*, 150, 148
 Holtzman J. A., et al., 2018, *AJ*, 156, 125
 Horta D., et al., 2020, *MNRAS*, 493, 3363
 Horta D., et al., 2021a, *MNRAS*, 500, 1385
 Horta D., et al., 2021b, *MNRAS*, 500, 5462
 Hughes M. E., Pfeffer J. L., Martig M., Reina-Campos M., Bastian N., Crain R. A., Kruijssen J. M. D., 2020, *MNRAS*, 491, 4012
 Ibata R. A., Gilmore G., Irwin M. J., 1994, *Nature*, 370, 194
 Ibata R. A., Lewis G. F., Martin N. F., 2016, *ApJ*, 819, 1
 Jönsson H., et al., 2018, *AJ*, 156, 126
 Jönsson H., et al., 2020, *AJ*, 160, 120
 Koch A., Grebel E. K., Martell S. L., 2019, *A&A*, 625, A75
 Koppelman H. H., Helmi A., Massari D., Price-Whelan A. M., Starkenburg T. K., 2019, *A&A*, 631, L9
 Kruijssen J. M. D., 2014, *Classical and Quantum Gravity*, 31, 244006
 Kruijssen J. M. D., 2015, *MNRAS*, 454, 1658
 Kruijssen J. M. D., Pelupessy F. I., Lamers H. J. G. L. M., Portegies Zwart S. F., Icke V., 2011, *MNRAS*, 414, 1339
 Kruijssen J. M. D., Maschberger T., Moeckel N., Clarke C. J., Bastian N., Bonnell I. A., 2012, *MNRAS*, 419, 841
 Kruijssen J. M. D., et al., 2020, *MNRAS*, 498, 2472
 Leung H. W., Bovy J., 2019a, *MNRAS*, 483, 3255
 Leung H. W., Bovy J., 2019b, *MNRAS*, 489, 2079
 Lind K., et al., 2015, *A&A*, 575, L12
 Mackereth J. T., Bovy J., 2018, *PASP*, 130, 114501
 Mackereth J. T., et al., 2017, *MNRAS*, 471, 3057
 Mackereth J. T., Crain R. A., Schiavon R. P., Schaye J., Theuns T., Schaller M., 2018, *MNRAS*, 477, 5072
 Mackereth J. T., et al., 2019, *MNRAS*, 482, 3426
 Majewski S. R., et al., 2017, *AJ*, 154, 94
 Martell S. L., Grebel E. K., 2010, *A&A*, 519, A14
 Martell S. L., et al., 2016, *ApJ*, 825, 146
 Massari D., et al., 2017, *MNRAS*, 468, 1249
 Masseron T., et al., 2019, *A&A*, 622, A191
 McMillan P. J., 2017, *MNRAS*, 465, 76
 Mészáros S., et al., 2015, *AJ*, 149, 153
 Mészáros S., et al., 2020, *MNRAS*, 492, 1641

- Myeong G. C., Vasiliev E., Iorio G., Evans N. W., Belokurov V., 2019, *MNRAS*, **488**, 1235
- Nataf D. M., et al., 2019, *AJ*, **158**, 14
- Nidever D. L., et al., 2015, *AJ*, **150**, 173
- Norris J. E., Yong D., Venn K. A., Gilmore G., Casagrande L., Dotter A., 2017, *ApJS*, **230**, 28
- Pfeffer J., Bastian N., Kruijssen J. M. D., Reina-Campos M., Crain R. A., Usher C., 2019, *MNRAS*, **490**, 1714
- Pfeffer J. L., Trujillo-Gomez S., Kruijssen J. M. D., Crain R. A., Hughes M. E., Reina-Campos M., Bastian N., 2020, *MNRAS*,
- Reina-Campos M., Hughes M. E., Kruijssen J. M. D., Pfeffer J. L., Bastian N., Crain R. A., Koch A., Grebel E. K., 2020, *MNRAS*, **493**, 3422
- Renzini A., Voli M., 1981, *A&A*, **500**, 221
- Robin A. C., Marshall D. J., Schultheis M., Reylé C., 2012, *A&A*, **538**, A106
- Robin A. C., Reylé C., Fliri J., Czekaj M., Robert C. P., Martins A. M. M., 2014, *A&A*, **569**, A13
- Savino A., Posti L., 2019, *A&A*, **624**, L9
- Schiavon R. P., et al., 2017, *MNRAS*, **465**, 501
- Schiavon R. P., Mackereth J. T., Pfeffer J., Crain R. A., Bovy J., 2020, in Bragaglia A., Davies M., Sills A., Vesperini E., eds, IAU Symposium Vol. 351, IAU Symposium. pp 170–173 ([arXiv:2002.08380](https://arxiv.org/abs/2002.08380)), [doi:10.1017/S1743921319007889](https://doi.org/10.1017/S1743921319007889)
- Shetrone M., et al., 2015, *ApJS*, **221**, 24
- Tang B., Liu C., Fernández-Trincado J. G., Geisler D., Shi J., Zamora O., Worthey G., Moreno E., 2019, *ApJ*, **871**, 58
- Tang B., Fernández-Trincado J. G., Liu C., Yu J., Yan H., Gao Q., Shi J., Geisler D., 2020, *ApJ*, **891**, 28
- Venn K. A., Irwin M., Shetrone M. D., Tout C. A., Hill V., Tolstoy E., 2004, *AJ*, **128**, 1177
- Ventura P., Di Criscienzo M., Carini R., D’Antona F., 2013, *MNRAS*, **431**, 3642
- Wilson J. C., et al., 2019, *PASP*, **131**, 055001
- Zamora O., et al., 2015, *AJ*, **149**, 181
- Zasowski G., et al., 2017, *AJ*, **154**, 198

APPENDIX A: TABLE OF APOGEE IDS FOR N-RICH STARS

Table A1 shows only the publicly available DR16 APOGEE ID’s, RA and DEC for the N-rich stars selected in this paper.

This paper has been typeset from a $\text{\TeX}/\text{\LaTeX}$ file prepared by the author.

Table A1. N-rich stars identified in the inner Galaxy.

APOGEE_ID	RA	DEC
2M16051144-2330557	241.297673	-23.515484
2M16180906-2442217	244.537768	-24.706036
2M16304650-2949522	247.693763	-29.831173
2M16314726-2945273	247.946932	-29.757591
2M16333703-3028333	248.404329	-30.475943
2M16335569-1344044	248.482062	-13.734557
2M17024730-2210387	255.697092	-22.177443
2M17271907-2718040	261.829481	-27.301126
2M17281699-3024573	262.070794	-30.415928
2M17285196-2013080	262.2165	-20.218908
2M17293012-3006008	262.375515	-30.100246
2M17293730-2725594	262.405434	-27.433182
2M17303980-2330234	262.665839	-23.506523
2M17305251-2651528	262.718823	-26.864672
2M17305645-3030155	262.73523	-30.504309
2M17325943-3034281	263.247636	-30.57449
2M17330999-1034023	263.291625	-10.567309
2M17333623-2548156	263.400967	-25.804361
2M17334418-3033313	263.434107	-30.558695
2M17334704-3034136	263.446029	-30.570456
2M17335209-3011013	263.467059	-30.183704
2M17340261-2616237	263.51091	-26.273256
2M17343807-2557555	263.658637	-25.965429
2M17350460-2856477	263.769185	-28.946587
2M17354063-3339547	263.919305	-33.665203
2M17404143-2714570	265.172631	-27.249172
2M17494963-2318560	267.4568	-23.315571
2M17504980-2255083	267.70754	-22.91898
2M17511127-3406383	267.796969	-34.110645
2M17523300-3027521	268.137518	-30.464495
2M17534571-2949362	268.44047	-29.826744
2M17552461-0122088	268.852559	-1.369136
2M17554454-2123058	268.93562	-21.384953
2M17555660-3238250	268.985848	-32.640282
2M17560439-3246181	269.01833	-32.771721
2M17571419-3328194	269.309144	-33.472073
2M17573951-2908334	269.414629	-29.142628
2M17595598-3117393	269.983287	-31.294264
2M18013879-2924112	270.411633	-29.403118
2M18014007-2649505	270.416966	-26.830719
2M18014786-2749080	270.449436	-27.818907
2M18015592-2749451	270.483011	-27.829222
2M18033529-2911240	270.897062	-29.19002
2M18035944-2908195	270.997669	-29.138758
2M18044803-2752467	271.200154	-27.879654
2M18050144-3005149	271.256017	-30.087484
2M18054875-3122407	271.453164	-31.377975
2M18061308-2522503	271.554505	-25.380655
2M18062975-2855357	271.623993	-28.926601
2M18072810-2459356	271.867096	-24.993229
2M18100924-3733319	272.538504	-37.55888
2M18101932-0930066	272.580527	-9.50184
2M18120031-1350169	273.001326	-13.838031
2M18121957-2926310	273.081553	-29.441954
2M18315425-2328124	277.976045	-23.470121
2M18334592-2903253	278.441366	-29.057034
2M18360807-2314389	279.033649	-23.244165
2M18364041-3402389	279.168375	-34.044147
2M18425902-3007370	280.74595	-30.126949
2M18442352-3029411	281.098036	-30.494764
2M18475308-2602331	281.971167	-26.042528
2M18562844-2814085	284.118507	-28.23572
2M18594405-3651518	284.933562	-36.864391
2M19175998-2919360	289.499952	-29.326691